Novel Human Lung Tissue Model for the Study of SARS-CoV-2 Entry, Inflammation and New Therapeutics

Judith Grau-Expósito[1]*, David Perea[1]*, Marina Suppi[1], Núria Massana[1], Ander Vergara[2], Maria José Soler[2], Javier García-Pérez[3], José Alcamí[3,4], Anna Serrano-Mollar[5,6], Joel Rosado[7], Vicenç Falcó[1], Meritxell Genescà[1]*, and Maria J. Buzon[1]*

[1]Infectious Diseases Department, Vall d'Hebron Research Institute (VHIR), Hospital Universitari Vall d'Hebron, Universitat Autònoma de Barcelona, Barcelona, Spain. VHIR Task Force COVID-19.

[2]Nephrology Research Department, Vall d'Hebron Research Institute (VHIR), Hospital Universitari Vall d'Hebron, Universitat Autònoma de Barcelona, Barcelona, Spain. VHIR Task Force COVID-19.

[3]AIDS Immunopathology Unit, National Center of Microbiology, Instituto de Salud Carlos III, Madrid, Spain.

[4]Clinic HIV Unit, Hospital Clinic, IDIBAPS, Barcelona, Spain.

[5]Experimental Pathology Department, Institut d'Investigacions Biomèdiques de Barcelona, Consejo Superior de Investigaciones Científicas (IIBB-CSIC), Institut d'Investigacions Biomèdiques August Pi i Sunyer (IDIBAPS), Barcelona, Spain.

[6]Centro de Investigaciones Biomédicas en Red de Enfermedades Respiratorias (CIBERES), Madrid, Spain.

[7]Thoracic Surgery and Lung Transplantation Department, Vall d'Hebron Institut de Recerca (VHIR), Hospital Universitari Vall d'Hebron, Barcelona, Spain. VHIR Task Force COVID-19.

Running title: Human lung for the study of SARS-CoV-2

Corresponding authors*: Maria J. Buzon (mariajose.buzon@vhir.org) and Meritxell Genescà (meritxell.genesca@vhir.org)

Abstract

The development of physiological models that reproduce SARS-CoV-2 infection in primary human cells will be instrumental to identify host-pathogen interactions and potential therapeutics. Here, using cell suspensions from primary human lung tissues (HLT), we have developed a platform for the identification of viral targets and the expression of viral entry factors, as well as for the screening of viral entry inhibitors and anti-inflammatory compounds. We show that the HLT model preserves its main cell populations, maintains the expression of proteins required for SARS-CoV-2 infection, and identifies alveolar type II (AT-II) cells as the most susceptible cell targets for SARS-CoV-2 in the human lung. Antiviral testing of 39 drug candidates revealed a highly reproducible system, and provided the identification of new compounds missed by conventional systems such as VeroE6. Using this model, we also show that interferons do not modulate ACE2 expression, and that stimulation of local inflammatory responses can be modulated by different compounds with antiviral activity. Overall, we present a novel and relevant physiological model for the study of SARS-CoV-2.

40 **Synopsis**

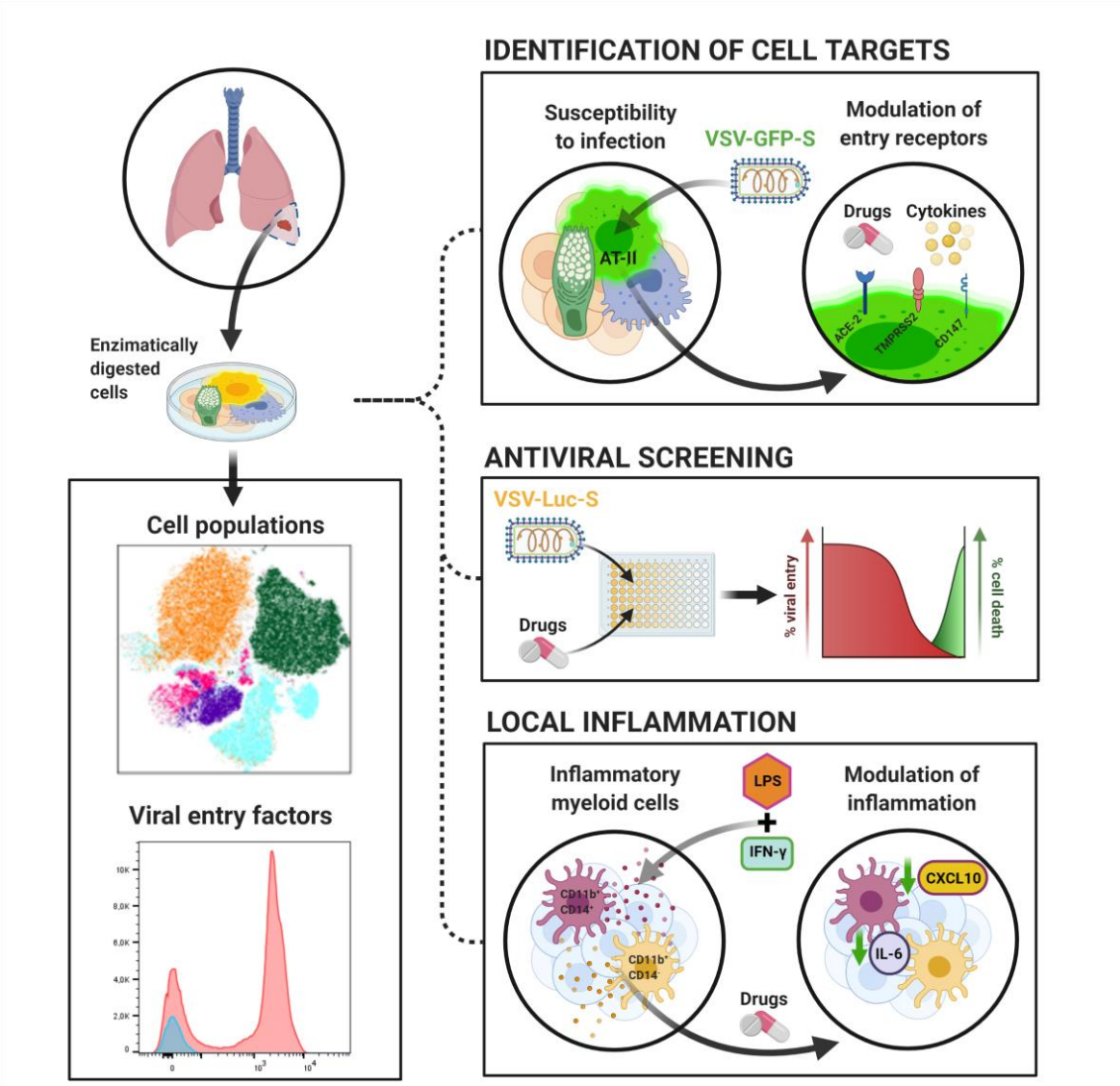

41

42 *Ex vivo* physiological systems for the study of SARS-CoV-2-host interactions are scarce. Here, we
43 establish a novel model using primary human lung tissue (HLT) for the analysis of cell tropism
44 and identification of therapeutics.

45 - The HLT model preserves main cell subpopulations, including alveolar type-2 cells,
46 and expression of SARS-CoV-2 entry factors ACE2, CD147, and TMPRSS2.
47 - The HLT model is readily susceptible to SARS-CoV-2 entry.
48 - Antiviral testing in the HLT model allows the identification of new candidates missed
49 by conventional systems.
50 - Local inflammation is supported in the HLT model and offers the identification of
51 relevant anti-inflammatory compounds for SARS-CoV-2 infection.

52 **Introduction**

53 We are facing a global health emergency, the COVID-19 pandemic, caused by the novel SARS-
54 CoV-2 virus. There is currently no specific treatment to cure SARS-CoV-2 infection to limit disease
55 progression of associated COVID-19. Early clinical trials showed promising drug candidates;
56 remdesivir, a compound that inhibits the RNA synthesis of SARS-CoV-2, was superior to placebo
57 in shortening the time to recovery in adults who were hospitalized with COVID-19 [1], however,
58 the *Solidarity* trial failed to support this observation [2]. Recently, plitidepsin, a molecule that
59 targets the eEF1A host protein has shown potent preclinical efficacy against SARS-CoV-2 [3].
60 Importantly, the development of *Acute Respiratory Distress Syndrome* in severe COVID-19
61 patients has been linked to dysregulated inflammatory responses. In this regard, the
62 glucocorticoid dexamethasone decreased 28-day mortality among patients receiving invasive
63 mechanical ventilation, but no benefit was observed in patients without respiratory support [4].
64 Thus, no effective treatment is currently available for COVID-19, and the rapid identification of
65 antivirals with the potential to be easily transferred into the clinic could save human lives.

66 Screening of novel drug candidates is often performed using cell lines. In this sense, the most
67 widely used cell lines for SARS-CoV-2 studies are epithelial cells derived either from lung (Calu-
68 3), kidney (VeroE6), or colon (CaCo-2) [5]. These immortalized systems are highly reproducible
69 and easy to handle but lack physiological relevance. The differential gene expression profiling of
70 cell lines compared with primary cells from tissues might significantly affect important enzymes
71 involved in the viral replication cycle. For instance, the level of ACE2 expression, the main
72 receptor used by SARS-CoV-2 for viral entry, is shown to be different in several cell lines [6],
73 while only a small fraction of alveolar type II (AT-II) cells, the main target for SARS-CoV-2 in the
74 lung, express ACE2 [7, 8]. In addition, SARS-CoV-2 spike (S) glycoprotein, which is responsible for
75 viral entry into target cells, can be activated by several host proteases, such as furin,
76 transmembrane serine proteinase 2 (TMPRSS2) and cathepsin L, in a pH-dependent or
77 independent manner [9, 10]. Whereas in some cell lines S protein is activated by endosomal pH-
78 dependent protease cathepsin L, in airway epithelial cells viral entry depends on the pH-
79 independent TMPRSS2 protease [10]. Thus, it is currently not well defined if SARS-CoV-2 may
80 utilize multiple cell-type-specific host proteins for viral replication in primary target tissues and
81 therefore, the potency of therapeutics directed against these proteins may also differ.

82 Further, inflammatory immune responses might also impact viral dynamics in the lung by
83 affecting the expression of entry receptors. In this sense, early studies discovered that ACE2 was
84 a human interferon-stimulated gene (ISG); IFN-β and IFN-γ were shown to strongly upregulate

85 the expression of ACE2 at the mRNA and cell surface protein levels, indicating that inflammatory
86 molecules could shape cell susceptibility to viral infection [11]. However, how anti-inflammatory
87 drugs may affect ACE2 expression and facilitate SARS-CoV-2 infection remains to be elucidated.
88 One study reported that the use of nonsteroidal anti-inflammatory drugs (NSAIDs), such as
89 ibuprofen, was linked to enhanced ACE2 expression in a diabetic-induced rat model [12] and
90 other reports raised alarms regarding the possible role of NSAIDs at increasing susceptibility to
91 SARS-CoV-2 infection [13, 14]. On the contrary, experimental and clinical evidence show that
92 medium-to-low-dose glucocorticoids may play a protective role in COVID-19 by activating ACE2
93 and suppressing the associated cytokine storm [15]. Overall, the use of more relevant and
94 physiological models for the study of either SARS-CoV-2 infection, the identification of drug
95 candidates, or the impact of new therapeutics on the disease could significantly advance the
96 successful translation of the results into the clinic.

97 Primary epithelial cell cultures of nasal and proximal airway epithelium have been used to study
98 SARS-CoV-2 infection in the upper airways [8, 16-18]. Similarly, organ on-chip and organoids
99 models of AT-II cells have been successfully developed [17, 19]. While very promising, these
100 models still miss certain aspects of cellular complexity present in primary tissues [20]. In this
101 regard, establishing a human lung tissue (HLT) model could offer a physiologically relevant
102 alternative to *in vitro* and *in vivo* approaches for several reasons; it mimics the main site of viral
103 replication in the lung, and contains all heterogeneous cell components present in the tissue
104 with greater functional complexity compared to cell lines. Although still representing a
105 reductionist *ex vivo* approach, it allows controlled experimental conditions. In the past, similar
106 lung models have been successfully established to study the effect of allergens and
107 inflammatory stimuli [21, 22]. Importantly, the HLT model allows mimicking an inflammatory
108 local response that could be attenuated by anti-inflammatory drugs [23]. Furthermore, it has
109 been used to provide low/medium throughput screening of anti-inflammatory candidate drugs
110 for the treatment of airway diseases [23]. Significantly, lung tissues not only can be infected with
111 SARS-CoV-2, but also generate local immune responses to viral infection [24]. Considering all
112 these factors, here we aimed to develop and characterize a physiological and reproducible
113 human lung tissue model, which could be used for the study of virus-host interactions,
114 identification of potential antiviral compounds, as well as help investigating the role of
115 inflammation in relation to SARS-CoV-2 infection.

116 ## Results

117 ### Characterization of the HLT model

118 To establish the HLT model, non-neoplastic areas from lung tissue resections were obtained
119 from hospitalized non-COVID19 patients undergoing thoracic surgery. First, we optimized cell
120 culture and digestion conditions, since the methodology used for tissue processing can
121 significantly impact viability and function of target cell populations. Thus, we tested the
122 preservation of AT-II, defined mainly by EpCAM and HLA-DR expression [25], and of several
123 hematopoietic cell subsets, after tissue digestion with different enzymes. Flow cytometry gating
124 strategy and cell markers used for identification of main populations are shown in **Figure S1A.**
125 We observed that collagenase outperformed liberase and trypsin at preserving AT-II cells, the
126 main SARS-CoV-2 target (**Figure S2A-B**). Among the hematopoietic cells present in the lung
127 tissue we identified CD3 T (which represented 1.94% ± 0.59 out of the total live cell fraction),
128 myeloid dendritic cells (0.03% ± 0.007), monocytes/macrophages subsets (0.42 ± 0.14%),
129 neutrophils (1.80% ± 0.53) and alveolar macrophages (0.05% ± 0.01). Moreover, non-
130 hematopoietic cells such as AT-II and endothelial cells represented 0.24% ± 0.05 and 0.5% ± 0.15
131 out of the total live cell fraction, respectively (**Figure 1A**). All populations have been previously
132 identified in human lungs [24, 26, 27]. Moreover, the nature of AT-II cells in lung cell suspensions
133 was confirmed by staining with phosphatase alkaline (**Figure 1B**), which has been shown to be a
134 reliable marker of type II cell phenotype both *in vitro* and *in vivo* [28]. Next, we focus on the
135 expression of previously identified proteins involved in viral entry. Single-cell transcriptome
136 studies have shown that ACE2, one of the main host cell surface receptors for SARS-CoV-2
137 attachment and infection, is predominantly expressed by AT-II cells [8, 29]. Moreover, ACE2
138 expression wanes in distal bronchiolar and alveolar regions paralleled by SARS-CoV-2 infectivity
139 [8]. In human parenchyma lung cells, we found ACE2 expression mainly in AT-II cells (**Figure 1C**),
140 a finding that was confirmed by immunohistochemistry (**Figure 1D**). Percentage of AT-II cells
141 expressing ACE2 was rather small and varied between individuals (6.29% ± 1.00) (**Figure 1C**), as
142 previously described [7]. We also studied the expression of CD147 on lung cells, which has been
143 reported as a novel route of SARS-CoV-2 infection *in vitro* and *in vivo* models [30]. CD147 was
144 ubiquitously expressed in several hematopoietic and non-hematopoietic cells (**Figure 1C**).
145 Importantly, 92.3% ± 1.14 of AT-II cells expressed CD147 (**Figure 1C**). Similarly, and in agreement
146 with other studies [31], TMPRSS2 protease expression was identified in AT-II cells (21.33% ±
147 7.52) (**Figure 1C**). Overall, we found that human lung suspensions preserved critical cell
148 populations and the expression of factors required for SARS-CoV-2 infection.

149 **Susceptibility of HLT cells to SARS-CoV-2 viral entry**

150 Next, we assessed if HLT cells were susceptible to viral infection. We generated pseudotyped
151 vesicular stomatitis virus (VSV) viral particles bearing the S protein of SARS-CoV-2 and expressing
152 either luciferase (VSV*ΔG (Luc)-S) or GFP (VSV*ΔG (GFP)-S) reporter genes upon cell entry. As a
153 control, we used the VSV-G virus, which has very broad cell tropism. As expected, VeroE6 cells
154 were highly susceptible to SARS-CoV-2 entry, as demonstrated for VSV*ΔG (GFP)-S and VSV-ΔG
155 (Luc)-S (**Figure 2A**). Anti-ACE2 antibody blocked more than 90% of VSV*ΔG (Luc)-S, but was
156 inactive for VSV-G (Luc) infection (**Figure 2B**). This observation has been widely reported before
157 [10, 32, 33], and identifies ACE2 as the main cell receptor required for viral entry in VeroE6.
158 Importantly for viral pathogenesis, it has been postulated that SARS-CoV-2 S protein might
159 downregulate ACE2 expression, as previously observed for SARS-CoV [34]. We consistently
160 observed a significant strong reduction in ACE2 expression after viral entry (**Figure 2C**).

161 We then evaluated the susceptibility of HLT cells to viral entry, using the same viral
162 constructs. HLT cells were readily infected with pseudotyped S particles (VSV*ΔG (Luc)-S and
163 VSV*ΔG (GFP)-S), with the natural donor variation representative of primary samples (**Figure**
164 **2D**). As expected [8], lung cells compatible with an AT-II phenotype were identified as the main
165 cell targets in steady conditions (**Figure 2E**). Blockade of ACE2 resulted in a donor-dependent
166 reduction of viral infectivity, ranging from 50 to 100% (**Figure 2F**). Camostat, a TMPRSS2
167 inhibitor, significantly inhibited viral entry in all HLT assays, although the entry process was not
168 always completely abrogated (**Figure 2F**), suggesting that AT-II cells may become infected
169 through the use of alternative factors [35]. Similarly, the presence of an anti-CD147 antibody
170 inhibited SARS-CoV-2 entry in AT-II cells (**Figure 2F**). Collectively, these data indicate that HLT
171 cells are highly susceptible to SARS-CoV-2 viral entry, and that ACE2, CD147 and TMPRSS2 are
172 important proteins for viral entry in human lung cells. Overall, these results support the value of
173 the HLT model to successfully study SARS-CoV-2 viral entry, and related mechanisms, in a more
174 physiological system.

175 **Antiviral assays in the HLT model**

176 To validate the HLT model as a platform for the screening of antiviral candidates, we assayed
177 potential antiviral compounds, most of them previously identified by computational methods
178 with predicted ability to inhibit SARS-CoV-2 cell entry due to their interaction with S protein or
179 with the interface S-ACE2 [36]. A detailed description of the 39 selected drugs is available in
180 **Table S1**. HLT cells were exposed to VSV*ΔG (Luc)-S virus in the presence of 1/5 serial dilution
181 of the different tested compounds. 20h post-exposure, antiviral activity and cell viability were

182 measured by luminescence. Results in HLT cells were systematically compared with antiviral
183 testing performed in the cell line VeroE6. Among 39 drugs that were evaluated in our study, 16
184 (41%) showed some antiviral activity against SARS-CoV-2 with EC_{50} values ranging from 0.5µM
185 to 66µM (**Table S2**). We observed that 23% of drugs had concordant results between both
186 models (**Figure 3**). Cepharanthine, a naturally occurring alkaloid reported to have potent anti-
187 inflammatory and antiviral properties, was one of the most potent antivirals identified in both
188 systems, with EC_{50} of 0.4µM and 6.1µM in VeroE6 and HLT cells, respectively (**Figure 3A and B**).
189 Of note, we observed cell toxicity at the highest concentrations ($CC_{50\ VeroE6}$= 22.3µM; $CC_{50\ HLT}$=
190 13.8µM), which translated in a satisfactory *selectivity index* (SI) in VeroE6 cells, but close to the
191 standard threshold of 2 in HLT cells (SI_{VeroE6} = 55.7; SI_{HLT} = 2.2) [37]. The anti-SARS-CoV-2 activity
192 of hydroxychloroquine, a compound known to interfere with endosomal acidification necessary
193 for the proteolytic activity of cathepsins, has been extensively reported [38, 39]. In our study,
194 we observed that hydroxychloroquine was equally effective at inhibiting viral entry in VeroE6
195 and HLT cells ($EC_{50\ VeroE6}$= 1.58µM; $EC_{50\ HLT}$= 9.26µM) (**Figure 3A, B**), with no apparent cytotoxicity
196 (**Figure 3C**). Ergoloid, an approved drug used for dementia, and recently identified as a potential
197 inhibitor of SARS-CoV-2 main protease [40], induced a ~90% viral entry inhibition in HLT cells at
198 non-toxic concentrations (**Figure 3A-C**). Indeed, *SI* for this compound was higher in the HLT
199 model than in VeroE6 cells (SI_{VeroE6} = 3.9; SI_{HLT} = 11.38). Similarly, ivermectin, a broad-spectrum
200 anti-parasitic compound, showed very similar antiviral potency in both models, however *SI*
201 greatly differed (SI_{VeroE6} = 1.4; SI_{HLT} = 8). Additionally, we also calculated the *Coefficient of*
202 *Variation (CV)* of the antiviral assays as a measure of relative variation in 50% Effective
203 Concentration (EC_{50}) values. We show that the *CV* varied from 0.9 to 15.36% in HLT cells (**Figure**
204 **3D**). The low *CV* obtained highlights the suitability of the HLT model for the identification of
205 antivirals.

206 We also detected discordant antiviral results between both models (**Figure 4**). Indeed, 5
207 drugs inhibited SARS-CoV-2 entry in HLT cells without affecting cell viability, but no effect was
208 observed in VeroE6 (**Figure 4A-C**). As expected, camostat, a TMPRSS2 inhibitor [41], was not
209 active in VeroE6 cells due to lack of TMPRSS2 expression in this cell line. However, camostat was
210 highly active in HLT cells (EC_{50}=2.7µM). Indeed, a clinical trial testing its potential to prevent
211 SARS-CoV-2 transmission is ongoing (NCT04625114). Further, sulindac, a nonsteroidal anti-
212 inflammatory drug, and valaciclovir, an antiviral drug, presented some inhibitory potential at
213 100 µM only in HLT cells. Interestingly, phenformin, an antidiabetic drug and an mTOR inhibitor,
214 has been postulated as an inhaled drug candidate against influenza and coronavirus infections
215 [42]. Phenformin reduced the incidence of influenza infection in diabetic patients during the

216 1971 outbreak [42]. Here, we observed that phenformin significantly reduced viral entry starting
217 at 4µM only in HLT cells, supporting previous recommendations as inhaled treatment. Finally,
218 eriodictyol, a flavonoid used as a medicinal plant [43], demonstrated certain activity at 20-
219 100µM. In contrast, luteolin induced potent viral entry suppression only in VeroE6 cells at high
220 concentrations (**Figure 4A-C**). Overall, these results indicate that the HLT is a reproducible and
221 highly relevant model for antiviral testing in a physiological system that recapitulates main
222 antiviral activities observed in cell models, and offers the identification of new compounds
223 missed by conventional systems.

224 **Impact of inflammation and anti-inflammatory drugs on ACE2 expression and SARS-CoV-2**
225 **viral entry**

226 Since SARS-CoV-2 viral infection rapidly induces an inflammatory response, we wondered if
227 certain components of this response could modulate ACE2 expression, potentially allowing
228 increased viral binding of SARS-CoV-2 and thus, enhancing infection. Further, ACE2 has been
229 previously identified as an ISG or a component of the IFN-signaling pathway [11, 44], and a
230 recent investigation showed that cultured human primary basal epithelial cells treated with IFN-
231 α2 and IFN-γ led to upregulation of ACE2 [11]. Moreover, IL-1β and IFN-β upregulated ACE2 in
232 large airway epithelial cell cultures [8]. Thus, considering that type I interferons represent a first
233 line of defence against viral infections and that several cytokines are rapidly induced and
234 associated with disease severity in COVID-19 patients [45], we tested the effects of different
235 molecules on ACE2 expression in our model. In initial experiments, we tested three different
236 doses of a wider range of molecules (including tumor necrosis factor (TNF), IL-6 and IFN-γ), which
237 were used to select doses and compounds of interest. Finally, the effect of IFN-α2, IFN-β1, IL-
238 1β, IL-10 and GM-CSF on ACE2 expression was evaluated in the HLT model. Cells were then
239 treated with selected immune stimuli and cultured for 20h, when the expression of ACE2 in AT-
240 II cells was evaluated by flow cytometry. The only significant change we observed was for IL-1β
241 stimulation, which decreased the fraction of AT-II cells expressing ACE2 (**Figure 5A**). No other
242 significant changes were observed. Overall, we show that relevant inflammatory stimuli have a
243 limited impact on ACE2 expression in AT-II cells, while the effect and impact of IL-1 β on viral
244 infection should be further explored.

245 It is currently not well documented if anti-inflammatory drugs could modulate ACE2
246 expression, and consequently, might impact susceptibility to SARS-CoV-2 infection [46]. Several
247 glucocorticoids have shown to impart activating effects on ACE2 expression in cell lines; cortisol
248 showed the strongest effect on ACE2 activation, followed by prednisolone, dexamethasone, and

249 methylprednisolone [15]. Moreover, NSAIDs, compounds that inhibit cyclooxygenase-1 and 2
250 mediating the production of prostaglandins, which play a role in inflammatory responses, have
251 been linked to ACE2 upregulation [15]. Here, we took advantage of our HLT model to study the
252 effect of several anti-inflammatory drugs on both ACE2 expression and SARS-CoV-2 viral entry.
253 1/5 dilutions of ibuprofen, cortisol, dexamethasone and prednisone were added to HLT cells for
254 20h. Overall, no effect on ACE2 expression was observed after the addition of these anti-
255 inflammatory drugs (**Figure 5B**). Consequently, the antiviral assay showed no major impact of
256 anti-inflammatory compounds on viral entry; however, high concentrations of prednisone and
257 dexamethasone showed a partial reduction of viral entry in HLT cells, without any apparent
258 impact on VeroE6 (**Figure 5C**). Thus, we show that selected anti-inflammatory drugs have limited
259 impact on ACE2 expression within AT-II cells present in the HLT model, as well as in SARS-CoV-2
260 viral entry.

261 **Anti-inflammatory properties of selected compounds**

262 Last, we were interested in modelling the anti-inflammatory properties of several drugs in
263 our HLT model. Based on their antiviral potency in HLT cells, we selected cepharanthine,
264 ergoloid, camostat, ivermectin, hydroxychloroquine and ciclesonide for further evaluation. Of
265 note, some of these drugs have been previously identified as immunomodulators with anti-
266 inflammatory effects (**Table S1**). However, their direct impact on inflammatory molecules
267 directly secreted by human lung cells has not been evaluated. HLT cells were stimulated with
268 lipopolysaccharides (LPS) and IFN-γ in the presence of these antivirals and, 20h after, the
269 expression of IL-6 and CXCL10, a potent pro-inflammatory cytokine and chemokine respectively,
270 was intracellularly measured by flow cytometry. As shown in **Figure 6A,** two major
271 subpopulations of myeloid cells contributed to the upregulation of CXCL10 and IL-6 expression
272 upon stimulation. Myeloid $CD11b^{+}CD14^{+}$ were the cells with a greater response, showing 50%
273 of cells expressing IL-6 and 30% expressing CXCL10 after stimulation (**Figure 6B**). Using this
274 model of local inflammation, we tested the capacity of the selected compounds to modify this
275 response. We observed that camostat had the most potent effect, which significantly reduced
276 the expression of CXCL10 in $CD11b^{+}CD14^{-}$ and of IL-6 in $CD11b^{+}CD14^{+}$ myeloid subsets (**Figure**
277 **6B**). Ergoloid, which has not been linked to modulation of inflammation before, significantly
278 reduced the expression of cytokines in $CD11b^{+}$ $CD14^{+}$ myeloid cells, and cepharantine reduced
279 IL-6 production from this subset. Finally, ciclesonide induced CXCL10 secretion in $CD11b^{+}CD14^{-}$
280 myeloid cells (**Figure 6B**). Altogether, our results validate the HLT model as a relevant method
281 for the identification of anti-inflammatory compounds impacting specific pro-inflammatory cell
282 populations from the lung parenchyma.

283 **Discussion**

284 The emergency created by the rapid spread of SARS-CoV-2 infection worldwide required a
285 quick response from physicians treating these patients, who adapted to the rapid knowledge
286 being generated by both clinical practice and basic research. However, up to date, no specific
287 drugs against SARS-CoV-2 have been approved for clinical use. In this sense, the choice of the
288 cell and animal models used to test the efficacy of antivirals will impact its rapid translation into
289 the clinics. Here, we have developed a novel human lung tissue (HLT) model that can be safely
290 performed in a BSL2 facility, which allows i) the identification of cell targets and expression of
291 viral entry factors, ii) the impact of inflammation on host-pathogen interactions and iii) a rapid
292 medium-high throughput drug screening of SARS-CoV-2 entry inhibitors and local anti-
293 inflammatory candidates.

294 While cell lines have been traditionally used for the screening of potential antiviral
295 compounds due to their reproducibility, as well as being quick and user-friendly assays, they lack
296 physiological relevance. Similarly, entry receptors and viral factors have been identified using
297 immortalized cell lines [10, 47], and cell targets for SARS-CoV-2 in tissues have been mainly
298 determined by analyzing the expression of viral entry factors in RNA-seq datasets [48] or using
299 replication-competent SARS-CoV-2 isolates in BSL3 facilities [49]. Importantly, these studies
300 have identified AT-II cells as main viral targets for SARS-CoV-2 infection in the lungs, and the
301 molecules ACE2, CD147 and TMPRSS2 as the main factors for viral entry [10, 30, 50]. However,
302 the development of more refined and translational *ex vivo* models of SARS-CoV-2 entry will not
303 only have implications for understanding viral pathogenesis, but also will be useful for the
304 characterization of cell targets under specific conditions and the identification of potential
305 antivirals blocking infection of primary cells. In our HLT model, the maintenance of cell type
306 complexity in their *in vivo* proportions may represent a significant advantage over previous
307 models [17, 19, 51]. Using pseudotyped viral particles expressing SARS-CoV-2 spike, we first
308 corroborated that AT-II cells are the primary cell target in lung tissue in steady conditions. This
309 agrees with several studies using different approximations [11, 52, 53] and validates our primary
310 model for viral tropism identification.

311 Moreover, we showed that the HLT model can be successfully used for drug screening
312 purposes. We tested 39 drugs and compared the results with antiviral testing in VeroE6 cells.
313 Not surprisingly, we showed discordant results between both models. Indeed, we found that
314 37.5% of the tested compounds had discordant results between HLT and VeroE6 cells; 31.25%
315 of drugs showed some antiviral effect in HLT but no activity was detected in VeroE6, and 6.2%

316 showed only antiviral effects in VeroE6 cells. Among other reasons, the differential expression
317 of several key proteins needed for viral entry, might explain current discrepancies between
318 models. Importantly, using the HLT model, we identified several compounds with antiviral
319 activity; cepharanthine showed an EC_{50} of 6.1µM and concordantly, it was recently identified in
320 a high throughput screening as one of the most potent drugs against SARS-CoV-2 [54], likewise
321 several other studies have pointed towards this drug as a potent entry and post-entry SARS-CoV-
322 2 inhibitor [55]. Instead, for hydroxychloroquine, an early report suggested no antiviral activity
323 in human lung cells due to different expression of the required proteases for viral entry [56]. In
324 our study, however, we observed that this drug was equally effective at inhibiting viral entry in
325 VeroE6 and HLT cells. Nevertheless, clinical trials failed to show effectiveness of this drug as a
326 treatment for COVID-19 [57-59]. Recently, a strong dependency of SARS-CoV-2 on TMPRSS2 for
327 viral entry, rather than on cathepsin L, was identified as a possible mechanistic explanation for
328 its failure *in vivo* [60]. Similarly, we identified ivermectin as an effective antiviral in HLT cells. Of
329 note, ivermectin received limited attention as a potential drug to be repurposed against COVID-
330 19 based on its limited ability to reach lung tissue *in vivo* [61]. Further, a clinical trial failed to
331 show a reduction in the proportion of PCR-positive patients seven days after ivermectin
332 treatment [62].

333 Importantly, the HLT model also provides a platform for testing anti-inflammatory drugs and
334 the modulation of viral entry factors with drug candidates and immunomodulatory stimuli. We
335 showed that IL-1β was able to reduce ACE2 expression in AT-II cells, in contrast to other
336 cytokines induced during SARS-CoV-2 infection like IFN-α2, IFN-β1, IL-10 and GM-CSF, which did
337 not impact ACE2 protein production. In primary epithelial cells derived from healthy nasal
338 mucosa, Ziegler et al. [11] showed a significant induction of ACE2 transcripts after IFN-α2 and
339 IFN-γ stimulation, as well as and in a human bronchial cell line treated with either type I or type
340 II IFN. Moreover, the authors showed that influenza A virus infection increased ACE2 expression
341 in lung resections [11], strongly suggesting that ACE2 was an ISG. However, following studies
342 showed that ACE2 transcription and protein production was not responsive to IFN. Instead, they
343 described a new RNA isoform, MIRb-ACE2, that was highly responsive to IFN stimulation, but
344 importantly, encoded a truncated and unstable protein product [63, 64]. These results highlight
345 the need to validate scRNA-seq data with orthogonal approaches, such as the confirmation of
346 protein expression levels in relevant systems. In the HLT model, we quantified ACE2 protein
347 expression and importantly, focused our analysis on AT-II cells, the main SARS-CoV-2 targets in
348 lung parenchyma. Also, in agreement with our results, a primary human bronchial epithelial cell
349 model, type I (β), II (γ), or III (λ1) IFNs did not induced ACE2 expression [65]. Moreover, a study

350 performed by Lang et al [66], showed that IFN-γ and IL-4 downregulate the SARS-CoV receptor
351 ACE2 in VeroE6 cells, and similarly, stimulation of A549 cells with IFN-α, IFN-γ, and IFN-α+IFN-γ
352 did not identify ACE2 as an ISG [67].

353 A feasible explanation for the increase of ACE2 protein production upon IL-1 β treatment is
354 that IL-1β activates disintegrin and metalloproteinase domain-containing protein 17 (ADAM17)
355 [68], which mediates the shedding of ACE2 [69]. Although this effect would seem positive to
356 reduce SARS-CoV-2 infection, ACE2 is a lung-protective factor, as it converts Angiotensin (Ang)
357 II to Ang-(1–7); while Ang II promotes harmful effects in the lung, e. g. fibrosis, vasoconstriction,
358 inflammation, endothelial dysfunction, edema, and neutrophil accumulation[70], Ang-(1-7) has
359 counter-regulatory effects protective of lung injury. Moreover, Ang-(1–7) plays an essential role
360 in hemostasis, as it favors anti-thrombotic activity in platelets [71]. In any case, treatment of
361 COVID-19 patients with respiratory insufficiency and hyper inflammation with IL-1 inhibitors was
362 associated with a significant reduction of mortality [72], indicating that at least during severe
363 COVID-19 the overall effect of IL-1β is detrimental. While the reduction of ACE2 expression in
364 AT-II cells by IL-1β may be of interest, it needs to be determined if in combination with other
365 cytokines rapidly induced during viral respiratory infection [73], this effect would remain.

366 Further, glucocorticoids and NSAIDS have been linked to ACE2 upregulation previously [15].
367 In contrast, we did not observe any significant impact of ibuprofen, cortisol, dexamethasone and
368 prednisone on ACE2 protein expression. These results are concordant with a recent report
369 showing that suppression of ciclooxigenase (COX)-2 by two commonly used NSAIDs, ibuprofen
370 and meloxicam, had no effect on ACE2 expression, viral entry, or viral replication in a mouse
371 model of SARS-CoV-2 infection [74]. Moreover, dexamethasone incompletely reduced viral
372 entry. This observation partially agrees with a study using lung cells previously treated with
373 dexamethasone, which showed significant suppression of SARS-CoV-2 viral growth [24].

374 In addition, we used the model for testing local inflammation and potential anti-
375 inflammatory drugs. Several resident and recruited myeloid subsets may contribute to the rapid
376 cytokine storm detected in COVID-19 patients [75-77]. Thus, the identification of antiviral drugs
377 that can also limit the extent of these initial pro-inflammatory events may offer added value to
378 the overall therapeutic effect of a given drug. In this sense, we observed that camostat
379 significantly reduced the expression of proinflammatory molecules IL-6 and CXCL10 in several
380 myeloid $CD11b^{+}$ subsets. Concordantly, in a previous study using primary cultures of human
381 tracheal epithelial cells infected with H1N1 virus, camostat also reduced the concentrations of
382 the cytokines IL-6 and TNF in cell supernatants [78], suggesting a potent anti-inflammatory

383 potential. In contrast, ivermectin did not affect the expression of cytokines in our model.
384 Differing from previous results, ivermectin was shown to have anti-inflammatory effects in mice
385 and *in vitro* using murine macrophages; ivermectin reduced the production of TNF, IL-1 and IL-
386 6, and suppressed LPS-induced NF-κB translocation[79]. Of note, our HLT model of inflammation
387 is optimized up to detect changes in the intracellular expression of cytokines by local myeloid
388 cells, and thus, how these intracellular changes reflect total cytokine production in supernatant
389 needs further evaluation.

390 Finally, it is also important to note the potential limitations of the model, including the limited
391 availability of human lung samples, inter-patient variation (age, smoking, etc.), the effects on
392 lung biology of the medical condition instigating surgery, and the location of the sample
393 resection which may affect the proportion of cell subsets such as AT-II. However, this variability
394 is what shapes the HLT into a highly physiological and relevant model in comparison to current
395 methods based on immortalized cell cultures. Besides the interest of the model proposed here,
396 our results highlight drugs with antiviral activity in HLT cells together with immunomodulatory
397 properties, which could increase the benefit of this treatment during COVID-19 disease
398 progression. For instance, camostat, cepharantine and ergoloid were three of the most potent
399 drugs inhibiting SARS-CoV-2 entry, and remarkably, also exerted a significant anti-inflammatory
400 effect on myeloid cells. Clinical trials with camostat, currently ongoing, ergoloid and
401 cepharatine, will shed light on their use as both antivirals and anti-inflammatory compounds.

402 **Materials and methods**

403 **Cells and virus**

404 VeroE6, isolated from kidney epithelial cells of an African green monkey, were grown in
405 DMEM medium supplemented with 10% fetal bovine serum (FBS; Gibco) 100 U/ml penicillin,
406 and 100 µg/ml streptomycin (Capricorn Scientific) (D10) and maintained at 37°C in a 5% CO_2
407 incubator.

408 The spike of the SARS-CoV-2 virus was generated (GeneArt Gene Synthesis, ThermoFisher
409 Scientific) from the codon-optimized sequence obtained by Ou et al.[35] and inserted into
410 pcDNA3.1D/V5-His-TOPO (pcDNA3.1-S-CoV2Δ19-G614). This plasmid presents the mutation
411 D614G and a deletion in the last 19 amino acids from the original spike. Pseudotyped viral stocks
412 of VSV*ΔG(Luc)-S were generated following the protocol described by Whitt [80] with some
413 modifications. Briefly, 293T cells were transfected with 3µg of the plasmid encoding the SARS-
414 CoV-2 spike. Next day, cells were infected with a VSV-G-Luc virus (MOI=1) (generated from a
415 lentiviral backbone plasmid that uses a VSV promoter to express luciferase) for 2h and gently
416 washed with PBS. Cells were incubated overnight in D10 supplemented with 10% of I1
417 hybridoma (anti-VSV-G) supernatant (ATCC CRL-2700) to neutralize contaminating
418 VSV*ΔG(Luc)-G particles. Next day, the resulting viral particles were collected and titrated in
419 VeroE6 cells by enzyme luminescence assay (Britelite plus kit; PerkinElmer), as described
420 previously [81].

421 **Lung tissue**

422 Lung tissues were obtained from patients without previous COVID-19 history and a recent
423 negative PCR test for SARS-CoV-2 infection undergoing thoracic surgical resection at the
424 Thoracic Surgery Service of the Vall d'Hebron University Hospital. Study protocol was approved
425 by the Ethical Committee (Institutional Review Board number PR(AG)212/2020). Non-neoplastic
426 tissue areas were collected in antibiotic-containing RPMI 1640 and immediately dissected into
427 approximately 8-mm^3 blocks. These blocks were first enzymatically digested with 5 mg/ml
428 collagenase IV (Gibco) and 100 µg/ml of DNase I (Roche) for 30 min at 37ºC and 400 rpm and,
429 then, mechanically digested with a pestle. The resulting cellular suspension was filtered through
430 a 70µm-pore size cell strainer (Labclinics) and washed twice with PBS. Pellet recovered after
431 centrifugation was resuspended in fresh medium (RPMI 1640 supplemented with 5% FBS, 100
432 U/ml penicillin, and 100 µg/ml streptomycin) and DNase I to dissolve cell aggregates, and the
433 resulting cell suspension was then filtered through a 40µm-pore size cell strainer (Labclinics).

434 Cell number and viability were assessed with LUNA™ Automated Cell Counter (Logos
435 Biosystems). For cell phenotyping the following antibodies were used: anti-CD31 (PerCP-Cy5.5,
436 BioLegend), anti-CD11b (FITC, BioLegend), anti-CD11c (Pe-Cy7, BD Biosciences), anti-E-cadherin
437 (Pe-CF594, BD Biosciences), primary goat anti-ACE2 (R&D systems), anti-CD14 (APC-H7, BD
438 Biosciences), anti-CD45 (AF700, BioLegend), anti-EpCAM (APC, BioLegend), anti-CD3 (BV650, BD
439 Biosciences), anti-CD15 (BV605, BD Biosciences) and anti-HLA-DR (BV421, BioLegend). For ACE2
440 detection, after surface staining, cells were stained with secondary donkey anti-goat IgG (PE,
441 R&D Systems) for 30 min at 4 ºC. Cell viability was determined using an AQUA viability dye for
442 flow cytometry (LIVE/DEAD fixable AQUA, Invitrogen). In some experiments, instead of CD11b
443 or CD15, we used a primary rabbit anti-TMPRSS2 or anti-CD147 (BV605, BD Biosciences),
444 respectively. For TMPRSS2 detection, after ACE2 staining with the appropriate secondary
445 antibody, cells were washed twice with PBS 1% NMS (normal mouse serum) and then stained
446 with a secondary goat anti-rabbit IgG (AF488, Thermofisher) for 30 min at 4ºC. After fixation
447 with PBS 2% PFA, cells were acquired in an LSR Fortessa (BD Biosciences), and data were
448 analyzed using the FlowJo v10.6.1 software (TreeStar).

449 **Cytospin and alkaline phosphatase staining**

450 Cytospin preparations were obtained from freshly isolated human lung cells at an
451 approximate density of 150,000 cells/slide, and air-dried during 15 min. Cells were stained with
452 alkaline phosphatase, as an enzyme marking epithelial type II cells, following manufacturer's
453 instructions (Alkaline phosphatase Kit, Sigma). The intensity of pink stain reflects the amount of
454 alkaline phosphatase in positive cells.

455 **ACE2 immunohistochemical staining in human lung tissue sections**

456 Human lungs were maintained in 10% formalin for 24 hours and then embedded in paraffin.
457 Paraffin-embedded lungs were cut into 4 µm sections. After removing the paraffin, endogenous
458 peroxidases were inactivated in an aqueous solution containing 3% H_2O_2 and 10% methanol and
459 antigen retrieval was performed heating the samples in citrate buffer (10mM citric acid, pH 6.0).
460 The sections were then blocked in bovine serum albumin (5%), incubated with anti-ACE2
461 antibody (R&D Systems cat. nº AF933, dilution 1:100) and with biotinylated secondary antibody
462 against goat IgGs (Vector Laboratories cat. nº BA-9500, dilution 1:250). Proteins were visualized
463 using the ABC Peroxidase Standard Staining Kit (ThermoFisher) followed by 3,3'-
464 Diaminobenzidine (DAB) Enhanced Liquid Substrate System (Sigma Aldrich). Counterstaining
465 was done with hematoxylin.

466 **Antiviral screening assay**

467 The complete list of compounds tested in this study, including information about its clinical
468 use, product reference and vendors is shown in **Table S1**. Duplicates of five-fold serial dilutions
469 of 39 antiviral compounds were tested in both VeroE6 cell line and in human lung tissue (HLT)
470 cells using at least 2 different donors. For VeroE6, five-fold serial dilutions of the compounds,
471 ranging from 100µM to 0,25nM, were prepared in D10 in a 96-well flat-bottom plates. VeroE6
472 cells were added at a density of 30.000 cells/well and incubated with the drug for at least 1 h
473 before infection. Subsequently, cells were infected with 1,500 $TCID_{50}$ of VSV*ΔG(Luc)-S virus. In
474 parallel, drug cytotoxicity was monitored by luminescence. To evaluate the antiviral activity of
475 drugs in HLT cells, five-fold serial dilutions of the compounds, ranging from 100µM to 0.8µM or
476 6.4nM, were prepared in R10 in a 96-well conic bottom plates. HLT cells were added at a density
477 of 300,000 cells/well and incubated with the compound for at least 1h before infection. Then,
478 MOI 0,1 of VSV*ΔG(Luc)-S virus were added to wells, and plates were spinoculated at 1,200g
479 and 37ºC for 2h. After infection, fresh medium was added to the wells and cell suspensions were
480 transferred into a 96-well round-bottom plate. Cells were then cultured overnight at 37°C in a
481 5% CO_2 incubator. Each plate contained the following controls: no cells (background control),
482 cells treated with medium (mock infection) and cells infected but untreated (infection control).
483 After 20h, cells were incubated with Britelite plus reagent (Britelite plus kit; PerkinElmer) and
484 then transferred to an opaque black plate. Luminescence was immediately recorded by a
485 luminescence plate reader (LUMIstar Omega). To evaluate cytotoxicity, we used the CellTiter-
486 Glo® Luminescent kit (Promega), following the manufacturer's instructions. Data was
487 normalized to the mock-infected control, after which EC_{50} and CC_{50} values were calculated using
488 Graph-Pad Prism 7.

489 **Modulation of ACE2 expression by anti-inflammatory drugs and immune stimuli**

490 VeroE6 and lung cells were incubated with five-fold serial dilutions of selected anti-
491 inflammatory compounds (ranging from 100µM to 0.8µM) for 20h. Tested drugs included
492 cortisol, ibuprofen, prednisone and dexamethasone. Lung cells were also incubated with the
493 following cytokines: GM-CSF (100 ng/ml, Immunotools), IL-1β (10 ng/ml, Immunotools), IL-10
494 (100 ng/ml, Immunotools), IFN-β (100 U/ml, Immunotools), or IFN-α2 (100 U/ml, Sigma Aldrich).
495 For determination of ACE2 expression, the following surface staining antibodies were used:
496 primary goat anti-ACE2 (R&D Systems), anti-CD45 (AF700, BioLegend), anti-EpCAM (APC,
497 BioLegend), and anti-HLA-DR (BV421, BioLegend). For ACE2 detection, cells were then stained
498 with secondary donkey anti-goat IgG (PE, R&D Systems) for 30 min at 4 ºC. A Fluorescent Minus

499 One control (FMO) without primary anti-ACE2 antibody was used as a control. Cell viability was
500 determined using an AQUA viability dye for flow cytometry (LIVE/DEAD fixable AQUA,
501 Invitrogen). After fixation with PBS 2% PFA, cells were acquired in an LSR Fortessa (BD
502 Biosciences) and analyzed using the FlowJo v10.6.1 software (TreeStar).

503 **Immunomodulatory capacity of selected drugs**

504 HLT cells were cultured in a round-bottom 96-well plate containing 20 µM of cepharanthine,
505 ergoloid mesylate, ciclesonide, hydroxychloroquine, ivermectin, or camostat mesylate alone or
506 in combination with the stimuli LPS (50 ng/ml) and IFN-γ (100 ng/ml). For each patient, a
507 negative control, cells treated with only medium, and a positive control, cells incubated in the
508 presence of LPS and IFN-γ, were included. Immediately, brefeldin A (BD Biosciences) and
509 monensin (BD Biosciences) were added to cells and cultured overnight at 37 ºC in 5% CO_2. Next
510 day, cellular suspensions were stained with the following antibodies: anti-CD11b (FITC,
511 BioLegend), anti-CD69 (PE-CF594, BD Biosciences), anti-CD14 (APC-H7, BD Biosciences), anti-
512 EpCAM (APC, BioLegend), anti-CD3 (BV650, BD Biosciences), anti-CD45 (BV605, BioLegend), and
513 anti-HLA-DR (BV421, BioLegend). Cells were subsequently fixed and permeabilized using the
514 Cytofix/Cytoperm™ kit (BD Biosciences) and intracellularly stained with anti-IL-6 (PE-Cy7,
515 BioLegend), and anti-CXCL10 (PE, BioLegend). Cell viability was determined using an AQUA
516 viability dye for flow cytometry (LIVE/DEAD fixable AQUA, Invitrogen). After fixation with PBS
517 2% PFA, cells were acquired in an LSR Fortessa (BD Biosciences), and data were analyzed using
518 the FlowJo v10.6.1 software (TreeStar).

519 **Statistical analyses**

520 Statistical analyses were performed with Prism software, version 6.0 (GraphPad). A P value
521 <0.05 was considered significant.

522 **Author contributions**

523 Conceptualization, MJ.B. and M.G.; Sample Collection, J.R.; Methodology J.G-E, D.P, M.S, N.
524 M, A.V, MJ.S, J.G-P, J.A, A.S.M and V.F; Formal Analysis, J.G-E., D.P, M.S, M.G and MJ.B; Writing-
525 Original Draft J.G-E and MJ.B; Writing- Review & Editing, J.G-E, M.G. and MJ.B; Funding
526 Acquisition, M.G and MJ.B.; all authors revised the manuscript; Supervision, M.G and MJ.B.

527 **Acknowledgments**

This work was primarily supported by a grant from the Health Department of the Government of Catalonia (DGRIS 1_5). This work was additionally supported in part by the Spanish Health Institute Carlos III (ISCIII, PI17/01470), the Spanish Secretariat of Science and Innovation and FEDER funds (grant RTI2018-101082-B-I00 [MINECO/FEDER]), the Spanish AIDS network Red Temática Cooperativa de Investigación en SIDA (RD16/0025/0007), the European Regional Development Fund (ERDF), the Fundació La Marató TV3 (grants 201805-10FMTV3 and 201814-10FMTV3), the Gilead fellowships GLD19/00084 and GLD18/00008 and the Becas Taller Argal 2020. M.J.B is supported by the Miguel Servet program funded by the Spanish Health Institute Carlos III (CP17/00179). N.M. is supported by a Ph.D. fellowship from the Vall d'Hebron Institut de Recerca (VHIR). The funders had no role in study design, data collection and analysis, the decision to publish, or preparation of the manuscript.

539 **References**

540 1. Beigel, J.H., et al., *Remdesivir for the Treatment of Covid-19 - Final Report.* N Engl J Med,
541 2020. **383**(19): p. 1813-1826.
542 2. Consortium, W.H.O.S.T., et al., *Repurposed Antiviral Drugs for Covid-19 - Interim WHO*
543 *Solidarity Trial Results.* N Engl J Med, 2021. **384**(6): p. 497-511.
544 3. White, K.M., et al., *Plitidepsin has potent preclinical efficacy against SARS-CoV-2 by*
545 *targeting the host protein eEF1A.* Science, 2021. **371**(6532): p. 926-931.
546 4. Group, R.C., et al., *Dexamethasone in Hospitalized Patients with Covid-19.* N Engl J Med,
547 2021. **384**(8): p. 693-704.
548 5. Takayama, K., *In Vitro and Animal Models for SARS-CoV-2 research.* Trends Pharmacol
549 Sci, 2020. **41**(8): p. 513-517.
550 6. Mossel, E.C., et al., *Exogenous ACE2 expression allows refractory cell lines to support*
551 *severe acute respiratory syndrome coronavirus replication.* J Virol, 2005. **79**(6): p. 3846-
552 50.
553 7. Ortiz, M.E., et al., *Heterogeneous expression of the SARS-Coronavirus-2 receptor ACE2 in*
554 *the human respiratory tract.* EBioMedicine, 2020. **60**: p. 102976.
555 8. Hou, Y.J., et al., *SARS-CoV-2 Reverse Genetics Reveals a Variable Infection Gradient in*
556 *the Respiratory Tract.* Cell, 2020. **182**(2): p. 429-446 e14.
557 9. Koch, J., et al., *Host Cell Proteases Drive Early or Late SARS-CoV-2 Penetration.* bioRxiv,
558 2020.
559 10. Hoffmann, M., et al., *SARS-CoV-2 Cell Entry Depends on ACE2 and TMPRSS2 and Is*
560 *Blocked by a Clinically Proven Protease Inhibitor.* Cell, 2020. **181**(2): p. 271-280 e8.
561 11. Ziegler, C.G.K., et al., *SARS-CoV-2 Receptor ACE2 Is an Interferon-Stimulated Gene in*
562 *Human Airway Epithelial Cells and Is Detected in Specific Cell Subsets across Tissues.* Cell,
563 2020. **181**(5): p. 1016-1035 e19.
564 12. Qiao, W., et al., *Ibuprofen attenuates cardiac fibrosis in streptozotocin-induced diabetic*
565 *rats.* Cardiology, 2015. **131**(2): p. 97-106.
566 13. Moore, N., et al., *Does Ibuprofen Worsen COVID-19?* Drug Saf, 2020. **43**(7): p. 611-614.
567 14. Kutti Sridharan, G., et al., *COVID-19 and Avoiding Ibuprofen. How Good Is the Evidence?*
568 Am J Ther, 2020. **27**(4): p. e400-e402.
569 15. Xiang, Z., et al., *Glucocorticoids improve severe or critical COVID-19 by activating ACE2*
570 *and reducing IL-6 levels.* Int J Biol Sci, 2020. **16**(13): p. 2382-2391.
571 16. Ravindra, N.G., et al., *Single-cell longitudinal analysis of SARS-CoV-2 infection in human*
572 *bronchial epithelial cells.* bioRxiv, 2020.
573 17. Si, L., et al., *Human organs-on-chips as tools for repurposing approved drugs as potential*
574 *influenza and COVID19 therapeutics in viral pandemics.* bioRxiv, 2020: p.
575 2020.04.13.039917.
576 18. Blanco-Melo, D., et al., *Imbalanced Host Response to SARS-CoV-2 Drives Development*
577 *of COVID-19.* Cell, 2020. **181**(5): p. 1036-1045 e9.
578 19. Lamers, M.M., et al., *An organoid-derived bronchioalveolar model for SARS-CoV-2*
579 *infection of human alveolar type II-like cells.* EMBO J, 2021. **40**(5): p. e105912.
580 20. Kim, J., B.K. Koo, and J.A. Knoblich, *Human organoids: model systems for human biology*
581 *and medicine.* Nat Rev Mol Cell Biol, 2020. **21**(10): p. 571-584.
582 21. Chang, Y., et al., *Upregulation of IL-17A/F from human lung tissue explants with cigarette*
583 *smoke exposure: implications for COPD.* Respir Res, 2014. **15**: p. 145.
584 22. Hackett, T.L., et al., *Oxidative modification of albumin in the parenchymal lung tissue of*
585 *current smokers with chronic obstructive pulmonary disease.* Respir Res, 2010. **11**: p.
586 180.
587 23. Rimington, T.L., et al., *Defining the inflammatory signature of human lung explant tissue*
588 *in the presence and absence of glucocorticoid.* F1000Res, 2017. **6**: p. 460.

24. Schaller, M.A., et al., *In vitro infection of human lung tissue with SARS-CoV-2: Heterogeneity in host defense and therapeutic response.* bioRxiv, 2021: p. 2021.01.20.427541.
25. Hasegawa, K., et al., *Fraction of MHCII and EpCAM expression characterizes distal lung epithelial cells for alveolar type 2 cell isolation.* Respir Res, 2017. **18**(1): p. 150.
26. Singer, B.D., et al., *Flow-cytometric method for simultaneous analysis of mouse lung epithelial, endothelial, and hematopoietic lineage cells.* Am J Physiol Lung Cell Mol Physiol, 2016. **310**(9): p. L796-801.
27. Baharom, F., et al., *Human Lung Mononuclear Phagocytes in Health and Disease.* Front Immunol, 2017. **8**: p. 499.
28. Katsumiti, A., et al., *Immortalisation of primary human alveolar epithelial lung cells using a non-viral vector to study respiratory bioreactivity in vitro.* Sci Rep, 2020. **10**(1): p. 20486.
29. Qi, F., et al., *Single cell RNA sequencing of 13 human tissues identify cell types and receptors of human coronaviruses.* Biochem Biophys Res Commun, 2020. **526**(1): p. 135-140.
30. Wang, K., et al., *CD147-spike protein is a novel route for SARS-CoV-2 infection to host cells.* Signal Transduct Target Ther, 2020. **5**(1): p. 283.
31. Qiao, Y., et al., *Targeting transcriptional regulation of SARS-CoV-2 entry factors ACE2 and TMPRSS2.* Proc Natl Acad Sci U S A, 2020.
32. Condor Capcha, J.M., et al., *Generation of SARS-CoV-2 Spike Pseudotyped Virus for Viral Entry and Neutralization Assays: A 1-Week Protocol.* Front Cardiovasc Med, 2020. **7**: p. 618651.
33. Fukushi, S., et al., *Vesicular stomatitis virus pseudotyped with severe acute respiratory syndrome coronavirus spike protein.* J Gen Virol, 2005. **86**(Pt 8): p. 2269-2274.
34. Kuba, K., et al., *A crucial role of angiotensin converting enzyme 2 (ACE2) in SARS coronavirus-induced lung injury.* Nat Med, 2005. **11**(8): p. 875-9.
35. Ou, X., et al., *Characterization of spike glycoprotein of SARS-CoV-2 on virus entry and its immune cross-reactivity with SARS-CoV.* Nat Commun, 2020. **11**(1): p. 1620.
36. Smith, M.D. and J.C. Smith, *Repurposing Therapeutics for COVID-19: Supercomputer-Based Docking to theSARS-CoV-2 Viral Spike Protein and Viral Spike Protein-Human ACE2 Interface.*
37. Suffness, M. and J. Pezzuto, *Methods in plant biochemistry: assays for bioactivity.* Academic Press, London, 1990: p. 71-133.
38. Yao, X., et al., *In Vitro Antiviral Activity and Projection of Optimized Dosing Design of Hydroxychloroquine for the Treatment of Severe Acute Respiratory Syndrome Coronavirus 2 (SARS-CoV-2).* Clinical Infectious Diseases, 2020. **71**(15): p. 732-739.
39. Maisonnasse, P. and J. Guedj, *Hydroxychloroquine use against SARS-CoV-2 infection in non-human primates.* 2020. **585**(7826): p. 584-587.
40. Alméciga-Díaz, C.J., et al., *Virtual Screening of Potential Inhibitors for SARS-CoV-2 Main Protease*. 2020, Preprints.org.
41. Hoffmann, M., et al., *Camostat mesylate inhibits SARS-CoV-2 activation by TMPRSS2-related proteases and its metabolite GBPA exerts antiviral activity.* bioRxiv, 2020.
42. Lehrer, S., *Inhaled biguanides and mTOR inhibition for influenza and coronavirus (Review).* World Acad Sci J, 2020. **2**(3).
43. Islam, A., et al., *The pharmacological and biological roles of eriodictyol.* Arch Pharm Res, 2020. **43**(6): p. 582-592.
44. Su, S. and S. Jiang, *A suspicious role of interferon in the pathogenesis of SARS-CoV-2 by enhancing expression of ACE2.* Signal Transduct Target Ther, 2020. **5**(1): p. 71.
45. Vabret, N., et al., *Immunology of COVID-19: Current State of the Science.* Immunity, 2020. **52**(6): p. 910-941.

640 46. Smart, L., et al., *A narrative review of the potential pharmacological influence and safety*
641 *of ibuprofen on coronavirus disease 19 (COVID-19), ACE2, and the immune system: a*
642 *dichotomy of expectation and reality.* Inflammopharmacology, 2020. **28**(5): p. 1141-
643 1152.
644 47. Shang, J., et al., *Cell entry mechanisms of SARS-CoV-2.* Proc Natl Acad Sci U S A, 2020.
645 **117**(21): p. 11727-11734.
646 48. Valyaeva, A.A., et al., *Expression of SARS-CoV-2 entry factors in lung epithelial stem cells*
647 *and its potential implications for COVID-19.* Sci Rep, 2020. **10**(1): p. 17772.
648 49. Kaufer, A.M., et al., *Laboratory biosafety measures involving SARS-CoV-2 and the*
649 *classification as a Risk Group 3 biological agent.* Pathology, 2020. **52**(7): p. 790-795.
650 50. Walls, A.C., et al., *Structure, Function, and Antigenicity of the SARS-CoV-2 Spike*
651 *Glycoprotein.* Cell, 2020. **183**(6): p. 1735.
652 51. Ogando, N.S., et al., *SARS-coronavirus-2 replication in Vero E6 cells: replication kinetics,*
653 *rapid adaptation and cytopathology.* J Gen Virol, 2020. **101**(9): p. 925-940.
654 52. Lukassen, S., et al., *SARS-CoV-2 receptor ACE2 and TMPRSS2 are primarily expressed in*
655 *bronchial transient secretory cells.* EMBO J, 2020. **39**(10): p. e105114.
656 53. Hamming, I., et al., *Tissue distribution of ACE2 protein, the functional receptor for SARS*
657 *coronavirus. A first step in understanding SARS pathogenesis.* J Pathol, 2004. **203**(2): p.
658 631-7.
659 54. Jeon, S., et al., *Identification of Antiviral Drug Candidates against SARS-CoV-2 from FDA-*
660 *Approved Drugs.* Antimicrob Agents Chemother, 2020. **64**(7).
661 55. Rogosnitzky, M., P. Okediji, and I. Koman, *Cepharanthine: a review of the antiviral*
662 *potential of a Japanese-approved alopecia drug in COVID-19.* Pharmacol Rep, 2020.
663 **72**(6): p. 1509-1516.
664 56. Hoffmann, M., et al., *Chloroquine does not inhibit infection of human lung cells with*
665 *SARS-CoV-2.* Nature, 2020. **585**(7826): p. 588-590.
666 57. Omrani, A.S., et al., *Randomized double-blinded placebo-controlled trial of*
667 *hydroxychloroquine with or without azithromycin for virologic cure of non-severe Covid-*
668 *19.* EClinicalMedicine, 2020. **29**: p. 100645.
669 58. Boulware, D.R., et al., *A Randomized Trial of Hydroxychloroquine as Postexposure*
670 *Prophylaxis for Covid-19.* N Engl J Med, 2020. **383**(6): p. 517-525.
671 59. Mitja, O., et al., *Hydroxychloroquine for Early Treatment of Adults with Mild Covid-19: A*
672 *Randomized-Controlled Trial.* Clin Infect Dis, 2020.
673 60. Ou, T., et al., *Hydroxychloroquine-mediated inhibition of SARS-CoV-2 entry is attenuated*
674 *by TMPRSS2.* PLoS Pathog, 2021. **17**(1): p. e1009212.
675 61. Bray, M., et al., *Ivermectin and COVID-19: A report in Antiviral Research, widespread*
676 *interest, an FDA warning, two letters to the editor and the authors' responses.* Antiviral
677 Res, 2020. **178**: p. 104805.
678 62. Chaccour, C., et al., *The effect of early treatment with ivermectin on viral load, symptoms*
679 *and humoral response in patients with non-severe COVID-19: A pilot, double-blind,*
680 *placebo-controlled, randomized clinical trial.* EClinicalMedicine, 2021. **32**: p. 100720.
681 63. Onabajo, O.O., et al., *Interferons and viruses induce a novel truncated ACE2 isoform and*
682 *not the full-length SARS-CoV-2 receptor.* Nat Genet, 2020. **52**(12): p. 1283-1293.
683 64. Ng, K.W., et al., *Tissue-specific and interferon-inducible expression of nonfunctional*
684 *ACE2 through endogenous retroelement co-option.* Nat Genet, 2020. **52**(12): p. 1294-
685 1302.
686 65. Busnadiego, I., et al., *Antiviral Activity of Type I, II, and III Interferons Counterbalances*
687 *ACE2 Inducibility and Restricts SARS-CoV-2.* mBio, 2020. **11**(5).
688 66. de Lang, A., A.D. Osterhaus, and B.L. Haagmans, *Interferon-gamma and interleukin-4*
689 *downregulate expression of the SARS coronavirus receptor ACE2 in Vero E6 cells.*
690 Virology, 2006. **353**(2): p. 474-81.

691 67. Russell, A.B., C. Trapnell, and J.D. Bloom, *Extreme heterogeneity of influenza virus*
692 *infection in single cells.* Elife, 2018. **7**.
693 68. Hall, K.C. and C.P. Blobel, *Interleukin-1 stimulates ADAM17 through a mechanism*
694 *independent of its cytoplasmic domain or phosphorylation at threonine 735.* PLoS One,
695 2012. **7**(2): p. e31600.
696 69. Heurich, A., et al., *TMPRSS2 and ADAM17 cleave ACE2 differentially and only proteolysis*
697 *by TMPRSS2 augments entry driven by the severe acute respiratory syndrome*
698 *coronavirus spike protein.* J Virol, 2014. **88**(2): p. 1293-307.
699 70. Domingo, P., et al., *The four horsemen of a viral Apocalypse: The pathogenesis of SARS-*
700 *CoV-2 infection (COVID-19).* EBioMedicine, 2020. **58**: p. 102887.
701 71. Fraga-Silva, R.A., et al., *The angiotensin-converting enzyme 2/angiotensin-(1-7)/Mas*
702 *receptor axis: a potential target for treating thrombotic diseases.* Thromb Haemost,
703 2012. **108**(6): p. 1089-96.
704 72. Cavalli, G., et al., *Interleukin-1 and interleukin-6 inhibition compared with standard*
705 *management in patients with COVID-19 and hyperinflammation: a cohort study.* Lancet
706 Rheumatol, 2021. **3**(4): p. e253-e261.
707 73. Liao, M., et al., *Single-cell landscape of bronchoalveolar immune cells in patients with*
708 *COVID-19.* Nat Med, 2020. **26**(6): p. 842-844.
709 74. Chen, J.S., et al., *Non-steroidal anti-inflammatory drugs dampen the cytokine and*
710 *antibody response to SARS-CoV-2 infection.* J Virol, 2021.
711 75. Zhang, D., et al., *COVID-19 infection induces readily detectable morphological and*
712 *inflammation-related phenotypic changes in peripheral blood monocytes, the severity of*
713 *which correlate with patient outcome.* medRxiv, 2020.
714 76. Fahlberg, M.D., et al., *Cellular events of acute, resolving or progressive COVID-19 in*
715 *SARS-CoV-2 infected non-human primates.* Nat Commun, 2020. **11**(1): p. 6078.
716 77. Aggarwal, N.R., L.S. King, and F.R. D'Alessio, *Diverse macrophage populations mediate*
717 *acute lung inflammation and resolution.* Am J Physiol Lung Cell Mol Physiol, 2014.
718 **306**(8): p. L709-25.
719 78. Yamaya, M., et al., *The serine protease inhibitor camostat inhibits influenza virus*
720 *replication and cytokine production in primary cultures of human tracheal epithelial*
721 *cells.* Pulm Pharmacol Ther, 2015. **33**: p. 66-74.
722 79. Zhang, X., et al., *Ivermectin inhibits LPS-induced production of inflammatory cytokines*
723 *and improves LPS-induced survival in mice.* Inflamm Res, 2008. **57**(11): p. 524-9.
724 80. Whitt, M.A., *Generation of VSV pseudotypes using recombinant DeltaG-VSV for studies*
725 *on virus entry, identification of entry inhibitors, and immune responses to vaccines.* J
726 Virol Methods, 2010. **169**(2): p. 365-74.
727 81. Li, M., et al., *Human immunodeficiency virus type 1 env clones from acute and early*
728 *subtype B infections for standardized assessments of vaccine-elicited neutralizing*
729 *antibodies.* J Virol, 2005. **79**(16): p. 10108-25.

730 **Figure legends**

731 **Figure 1. Phenotyping of human lung cells.** (**A**). *t*-distributed Stochastic Neighbor
732 Embedding (t-SNE) representation displaying the major cell clusters present in the $CD45^+$ and
733 $CD45^-$ $EpCam^+$ fractions of a representative human lung tissue. The vertical bars in the right panel
734 show the frequency of each subset relative to live cells. All cell subsets were identified as shown
735 in Figure S1A. mDCs, myeloid dendritic cells; AT-II, alveolar type 2. (**B**). Phosphatase alkaline
736 positive AT-II cells (pink staining) were detected in a cytospin obtained from human lung tissue
737 cells and observed at 10x. Lower panel shows a high magnification (40x) of the black square.
738 Scale bars are 100 µm and 10 µm in top and bottom panels, respectively. (**C**). *t*-distributed
739 Stochastic Neighbor Embedding (tSNE) representation for ACE2, CD147 and TMPRSS2
740 expression in $CD45^+$ and $CD45^-EpCam^+$ fractions from a representative lung tissue. Right graphs
741 show the percentage of expression of each entry factor in the different cell subpopulations,
742 which were identified as in Figure 1A with some modifications for the identification of myeloid
743 cells and neutrophils (From big cells: monocytes/macrophages, $CD11c^+$HLA-DR^+ $CD14^+$; Alveolar
744 macrophages and mDCs, $CD11c^+$ HLA-DR^+ $CD14^-$; Neutrophils, $CD11c^-$ HLA-DR^- $CD14^-$ $CD3^-$). (**D**).
745 Images of ACE2 immunohistochemical staining in human lung tissue sections at 40x
746 magnification, counterstained with haematoxylin (top) or without (bottom). Black arrows
747 indicate staining of ACE2 in AT-II cells (upper panel). Mean±SEM is shown for all graphs.

748 **Figure 2. Susceptibility of VeroE6 and the HLT model to SARS-CoV-2 viral entry.** VeroE6 and
749 HLT cells were infected with two different viral constructs (GFP and Luciferase) expressing the
750 spike protein upon viral entry; VSV*ΔG(GFP)-Spike and VSV*ΔG(Luc)-Spike. (**A**) Representative
751 flow cytometry plots of VeroE6 cells infected with VSV*ΔG(GFP)-Spike or the background form
752 VSV*ΔG(GFP)-empty (left panel); and luciferase activity (RLUs; relative light units) at 20h post-
753 infection with the pseudotyped VSV*G(Luc)-G, the VSV*ΔG(Luc)-Spike or the background form
754 VSV*ΔG(Luc)-empty (right panel). (**B**) Percentage of viral entry after treatment with anti-ACE2
755 antibody (10µg/ml) in VeroE6 cells infected with the pseudotyped virus expressing the control
756 G protein or the spike from SARS-CoV-2. (**C**) A flow cytometry plot showing ACE2 expression in
757 GFP^+ VeroE6 cells. Right graph shows mean fluorescence intensity (MFI) of ACE2 in both infected
758 and uninfected fractions, based on GFP expression. (**D**) Representative flow cytometry plots of
759 HLT cells infected with the viral construct expressing the spike protein (VSV*ΔG(GFP)-Spike) or
760 the background form (VSV*ΔG(GFP)-empty) (left panel); and luciferase activity (RLUs; relative
761 light units) at 20h post-infection with the VSV*ΔG(Luc)-Spike or the background form
762 VSV*ΔG(Luc)-empty (right panel). Infection was measured as the percentage of GFP or RLUs,
763 respectively. (**E**) Susceptible HLT cells to viral entry (identified as GFP^+ cells) compatible with an

764 AT-II phenotype, determined by the co-expression of HLA-DR and EpCAM in the $CD45^-CD31^-$
765 fraction of live cells. (**F**) Bar plots showing the percentage of viral entry inhibition un HLT cells in
766 the presence of anti-ACE2 antibody (15µg/ml), camostat (100µM) or anti-CD147 antibody
767 (25µg/ml) after cell challenge with VSV*ΔG(Luc)-Spike (left graph) or VSV*ΔG(GFP)-Spike (right
768 graph). Mean±SEM is shown for all graphs. Data in panel 2C were analyzed by a Wilcoxon
769 matched-pairs test; *p<0,05.

770 **Figure 3. Antiviral assays with concordant results between models**. (**A**). Percentage of viral
771 entry in VeroE6 and HLT cells exposed to VSV*ΔG(Luc)-Spike in the presence of cepharanthine,
772 ergoloid, hydroxychloroquine, hypericin, licofelone, ivermectin, ciclesonide, quercitin,
773 vidarabine and celecoxib. Drugs were used at concentrations ranging from 100µM to 0.256nM,
774 in VeroE6, and to 0.8µM in lung cells. Non-linear fit model with variable response curve from at
775 least two independent experiments in replicates is shown (red lines). Cytotoxic effect on VeroE6
776 cells and HLT exposed to drug concentrations in the absence of virus is also shown (green lines).
777 (**B**). EC_{50} values of each drug in VeroE6 and HLT cells. (**C**). CC_{50} values of each drug are shown for
778 VeroE6 and for HLT cells. (**D**). EC_{50}'s coefficient of variation was calculated for ergoloid,
779 hydroxychloroquine and cepharanthine in the HLT model. Data includes two independent
780 experiments using different donors in replicates.

781 **Figure 4. Antiviral assays with discordant results between models**. (**A**). Percentage of viral
782 entry in VeroE6 and HLT cells exposed to VSV*ΔG(Luc)-Spike in the presence of luteolin,
783 eriodictyol, phenformin, camostat, sulindac, and valaciclovir. Drugs were used at concentrations
784 ranging from 100µM to 0.256 nM, in VeroE6, and to 0.8µM in lung cells. Non-linear fit model
785 with variable response curve from at least two independent experiments in replicates is shown
786 (red lines). Cytotoxic effect on VeroE6 cells and HLT exposed to drug concentrations in the
787 absence of virus is also shown (green lines). (**B**). EC_{50} values of each drug in VeroE6 and HLT cells.
788 (**C**)**.** CC_{50} values of each drug are shown for VeroE6 and HLT cells.

789 **Figure 5. Impact of inflammation and anti-inflammatory drugs on SARS-CoV-2 viral entry**
790 **and ACE2 expression.** Both models, HLT cells and VeroE6 cells, were incubated in the presence
791 of different anti-inflammatory drugs to evaluate the modulation of ACE2 expression by flow
792 cytometry and the antiviral effect by luminescence. (**A**). HLT cells were treated with different
793 stimuli for 20h and the percentage of protein expression (left) or the mean fluorescence
794 intensity (MFI, right) of ACE2 receptor was evaluated in the AT-II fraction by flow cytometry. (**B**)
795 Modulation of ACE2 protein expression was assessed by flow cytometry in both models, Vero
796 E6 and HLT cells, in the presence of different concentrations of each anti-inflammatory drug,

797 ranging from 100µM to 0.8µM. Percentage of ACE2 expression was quantified in AT-II cells from
798 at least six independent lung samples, and in VeroE6 cells from 2 independent experiments. (**C**).
799 Cytotoxic effect on Vero E6 and HLT cells exposed to VSV*ΔG(Luc)-Spike in the presence of
800 different concentrations of the anti-inflammatory drugs prednisone, cortisol, ibuprofen and
801 dexamethasone. Drugs were used at a concentration ranging from 100µM to 0.256 nM, in
802 VeroE6, and to 0.8µM in lung cells. Non-linear fit with variable response curve from at least two
803 experiments in replicates is shown (red lines). Cytotoxic effect on Vero E6 cells and HLT cells
804 exposed to different concentrations of drugs in the absence of virus is also shown (green lines).
805 Mean±SEM are shown and statistical comparisons with the control medium were performed
806 using the Wilcoxon test. *p<0.05.

807 **Figure 6. Anti-inflammatory effect of compounds with antiviral activity against SARS-CoV-**
808 **2.** HLT cells were cultured in the presence of 20µM of cepharanthine, ergoloid mesylate,
809 ciclesonide, hydroxychloroquine sulfate, ivermectin or camostat mesylate, alone or in
810 combination with the stimuli LPS (50 ng/ml) and IFN-γ (100 ng/ml). (**A**) *t*-distributed Stochastic
811 Neighbor Embedding (t-SNE) representations displaying the major cell clusters present in live
812 $CD45^+$ myeloid gate, based on FSC and SSC, of a representative human lung tissue in baseline
813 conditions and after stimulation with LPS and IFN-γ. Two major subsets of myeloid cells are
814 shown ($CD11b^+$ $CD14^+$, in blue-green, and $CD11b^+$ $CD14^-$, in orange). The expression of CXCL10
815 and IL-6 among the different populations is shown in maroon and green, respectively. (**B**)
816 Expression of CXCL10 and IL-6 was measured in HLT cells in response to stimuli in the presence
817 of selected drugs in both myeloid subpopulations, $CD11b^+$ $CD14^+$ (left panel) and $CD11b^+$ $CD14^-$
818 (right panel). HQ, hydroxychloroquine. Mean±SEM are represented and statistical comparisons
819 with the control medium were performed using the One sample t test. *p<0.05, **p<0.01.

820 **Figure S1. Gating strategy for the identification of cell subpopulations in the human lung**
821 **tissue model**. (**A**) General gating strategy used to identify different cell subsets in lung samples.
822 A gate based on FSC vs. SSC was followed by doublet and dead cells exclusion. From live $CD45^-$
823 cells, endothelial cells ($CD31^+$, purple) and epithelial cells ($EpCAM^+$, grey) were gated, and within
824 epithelial cells, AT-II cells ($EpCAM^+$ and $HLA\text{-}DR^+$, pink) were identified. Out of live $CD45^+$ cells
825 and based on FSC vs. SSC, we identified a lymphocyte population in which we distinguished
826 between non-T lymphocytes (turquoise) and T cells (dark green) based on CD3 expression; and
827 big cells, where we identified three major subsets based on their expression of CD11b and CD11c
828 and, subsequently, CD14 and HLA-DR markers. We identified alveolar macrophages (blue),
829 monocytes (violet), myeloid dendritic cells (mDCs, fuchsia) and neutrophils (orange). (**B**)

830 Representative flow cytometry plots showing ACE2 staining and its respective fluorescence
831 minus one (FMO) control.

832 **Figure S2. Optimization of lung tissue enzymatic digestion visualized by *t*-distributed**
833 **Stochastic Neighbor Embedding (tSNE).** (**A**) Representative tSNE maps showing concatenated
834 flow cytometry standard files for three different protocols based on different digestion enzymes
835 (collagenase, liberase or trypsin) from total live cells (upper), $CD45^+$ cells (middle) and $CD45^-$ cells
836 (lower). (**B**) Bar plots showing cell-type composition (count) analyzed by flow cytometry for each
837 tissue protocol.

838 **Figure S3. Gating strategy for the identification of anti-inflammatory effects of selected**
839 **compounds.** (**A**) General gating strategy used to evaluate the expression of inflammatory
840 molecules in lung samples. A gate based on FSC vs. SSC was followed by doublet and dead cells
841 exclusion. From live $CD45^+$ cells and based on FSC vs. SSC, we identified lymphocyte population
842 and big cells, in which we identified two subsets based on their expression of CD11b and CD14:
843 myeloid $CD11b^+CD14^+$ cells (blue-green) and myeloid $CD11b^+CD14^-$ cells (orange) are shown.

Figure 1

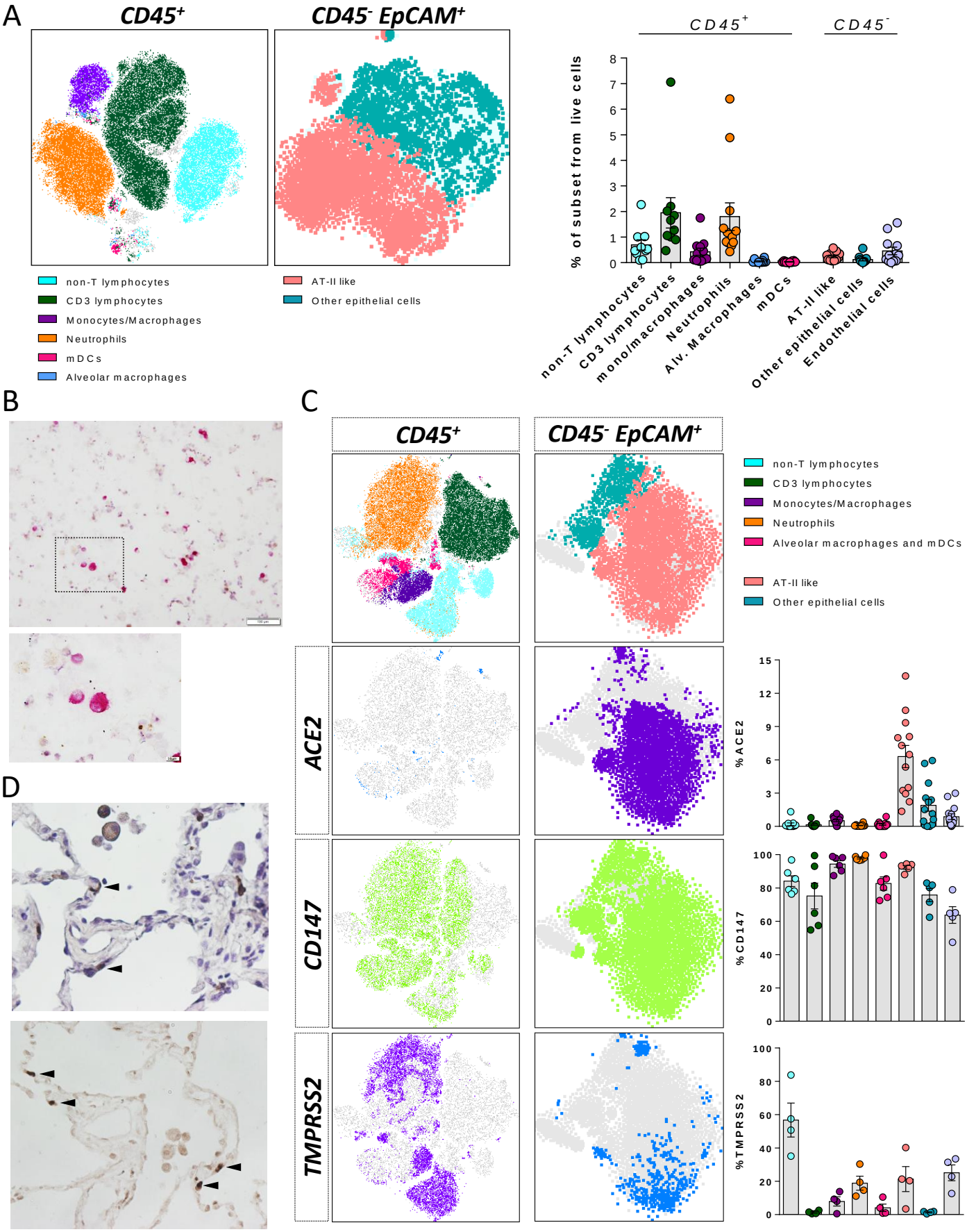
A
CD45+
CD45- EpCAM+
non-T lymphocytes
CD3 lymphocytes
Monocytes/Macrophages
Neutrophils
mDCs
Alveolar macrophages
AT-II like
Other epithelial cells
CD45+
CD45-
% of subset from live cells
non-T lymphocytes
CD3 lymphocytes
mono/macrophages
Neutrophils
Alv. Macrophages
mDCs
AT-II like
Other epithelial cells
Endothelial cells
B
C
CD45+
CD45- EpCAM+
non-T lymphocytes
CD3 lymphocytes
Monocytes/Macrophages
Neutrophils
Alveolar macrophages and mDCs
AT-II like
Other epithelial cells
ACE2
% ACE2
CD147
% CD147
TMPRSS2
% TMPRSS2
D

Figure 2

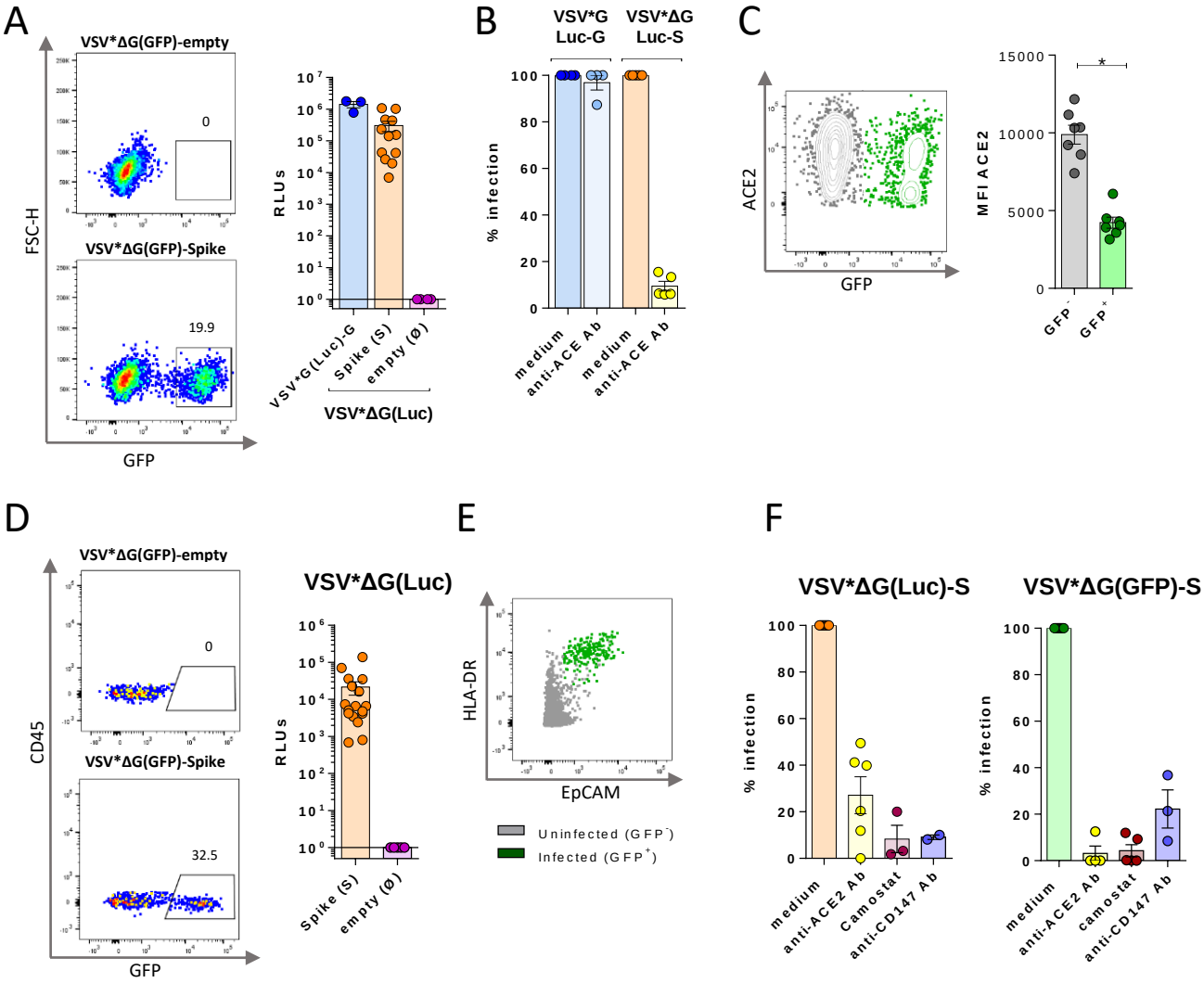
A
VSV*ΔG(GFP)-empty
0
VSV*ΔG(GFP)-Spike
19.9
FSC-H
GFP
RLUs
VSV*G(Luc)-G
Spike (S)
empty (Ø)
VSV*ΔG(Luc)
B
VSV*G Luc-G
VSV*ΔG Luc-S
% infection
medium
anti-ACE Ab
medium
anti-ACE Ab
C
ACE2
GFP
MFI ACE2
15000
10000
5000
0
*
GFP⁻
GFP⁺
D
VSV*ΔG(GFP)-empty
0
VSV*ΔG(GFP)-Spike
32.5
CD45
GFP
VSV*ΔG(Luc)
RLUs
Spike (S)
empty (Ø)
E
HLA-DR
EpCAM
Uninfected (GFP⁻)
Infected (GFP⁺)
F
VSV*ΔG(Luc)-S
VSV*ΔG(GFP)-S
% infection
medium
anti-ACE2 Ab
Camostat
anti-CD147 Ab
medium
anti-ACE2 Ab
camostat
anti-CD147 Ab

Figure 3

A

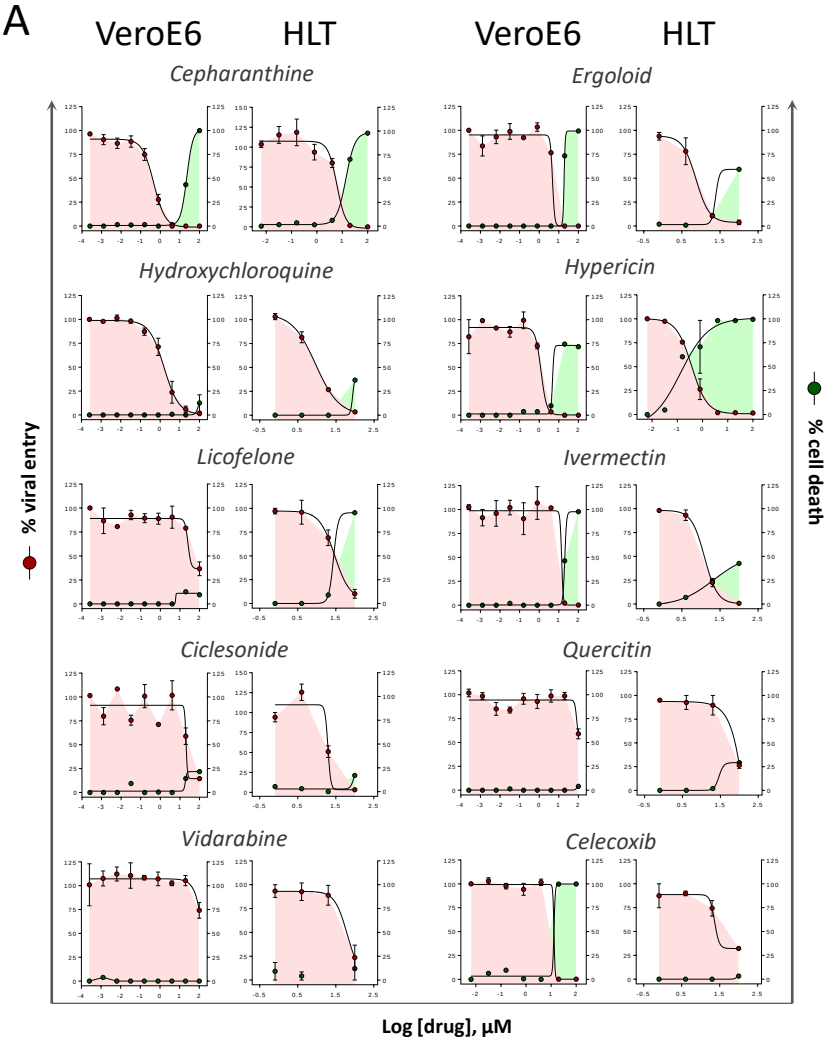

B

	VeroE6	HLT
Drugs	EC_{50} (µM)	
Cepharanthine	0.4	6.1
Quercitin	>100	78
Ergoloid	4.7	7.7
Ciclesonide	20.5	19.6
Licofelone	87.5	29.3
Hydroxychloroquine	1.58	9.2
Ivermectin	13.9	12.4
Hypericin	1.2	0.37
Vidarabine	>100	66
Celecoxib	13	~25

C

	VeroE6	HLT
Drugs	CC_{50} (µM)	
Cepharanthine	22.3	13.8
Quercitin	>100	>100
Ergoloid	18.6	~87.7
Ciclesonide	>100	>100
Licofelone	>100	29.4
Hydroxychloroquine	>100	>100
Ivermectin	20.23	>100
Hypericin	4.8	0.13
Vidarabine	>100	>100
Celecoxib	13	>100

D

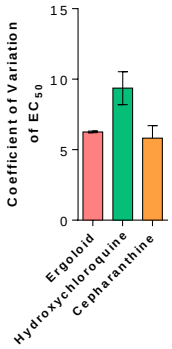

Figure 4

A

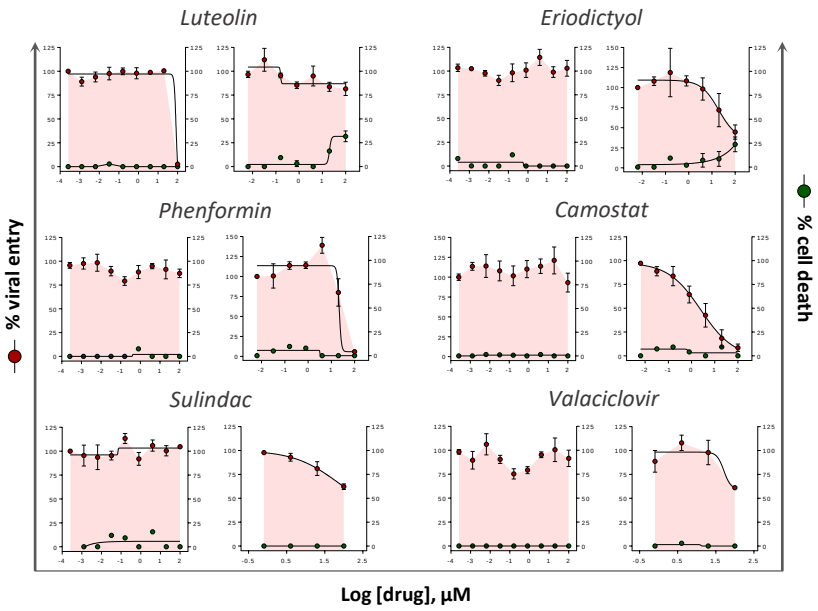

B

	VeroE6	HLT
Drugs	EC_{50} (µM)	
Eriodictyol	no effect	90
Luteolin	~70.7	no effect
Camostat	no effect	2.7
Phenformin	no effect	~22.45
Sulindac	no effect	>100
Valaciclovir	no effect	>100

C

	VeroE6	HLT
Drugs	CC_{50} (µM)	
Eriodictyol	>100	>100
Luteolin	>100	>100
Camostat	>100	>100
Phenformin	>100	>100
Sulindac	>100	>100
Valaciclovir	>100	>100

Figure 5

A

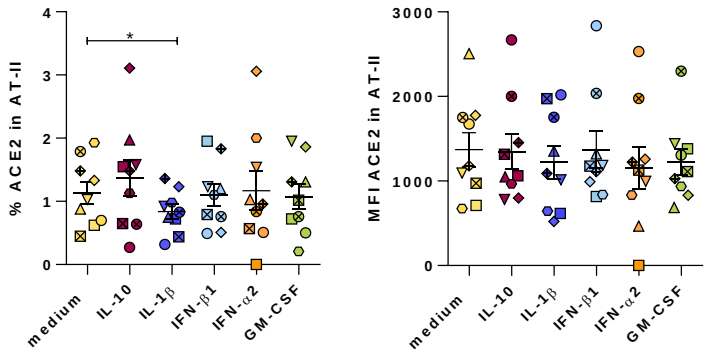
% ACE2 in AT-II
MFI ACE2 in AT-II
medium
IL-10
IL-1β
IFN-β1
IFN-α2
GM-CSF

B

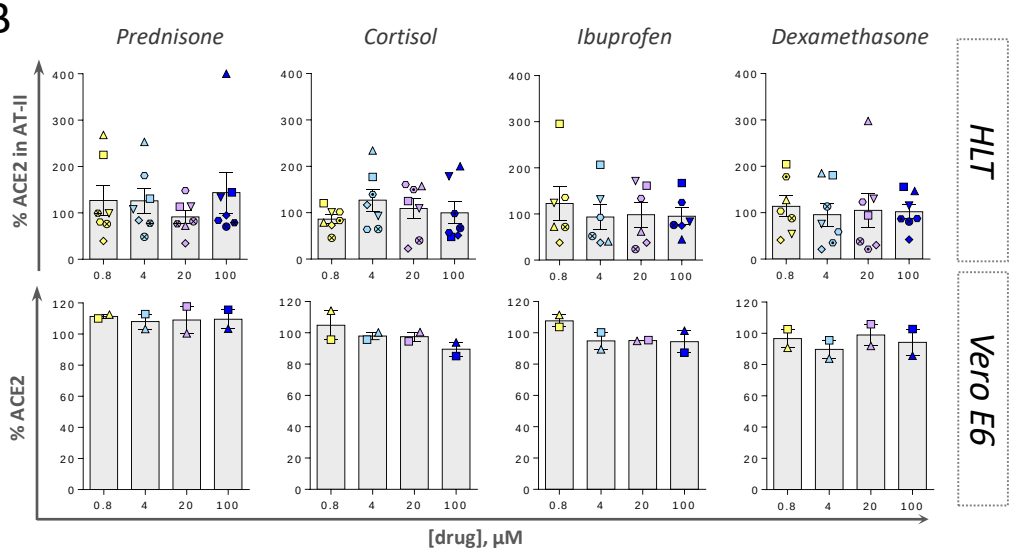
Prednisone
Cortisol
Ibuprofen
Dexamethasone
% ACE2 in AT-II
% ACE2
HLT
Vero E6
[drug], µM

C

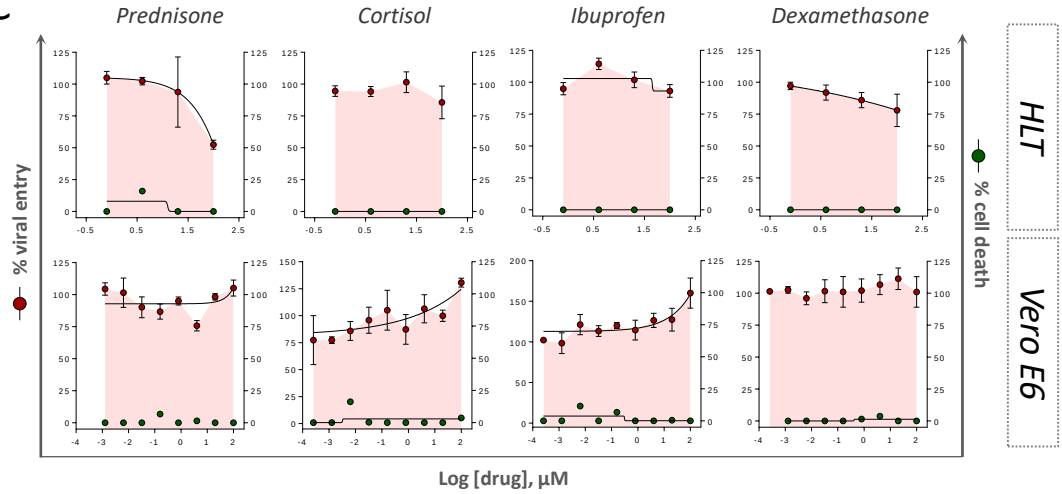
Prednisone
Cortisol
Ibuprofen
Dexamethasone
% viral entry
% cell death
HLT
Vero E6
Log [drug], µM

Figure 6

A

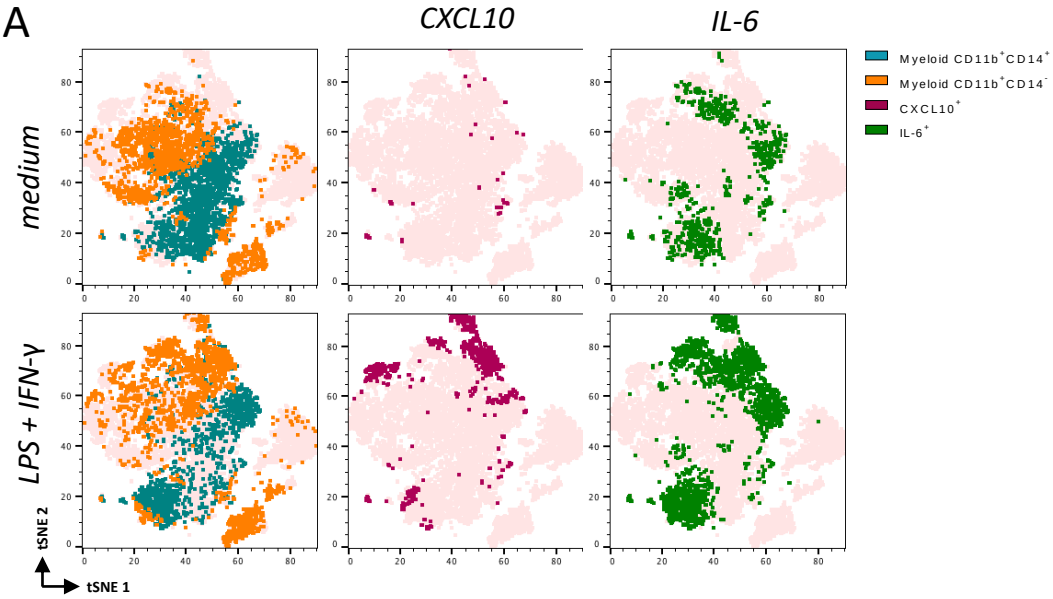
CXCL10
IL-6
medium
LPS + IFN-γ
Myeloid CD11b+CD14+
Myeloid CD11b+CD14-
CXCL10+
IL-6+
tSNE 2
tSNE 1

B

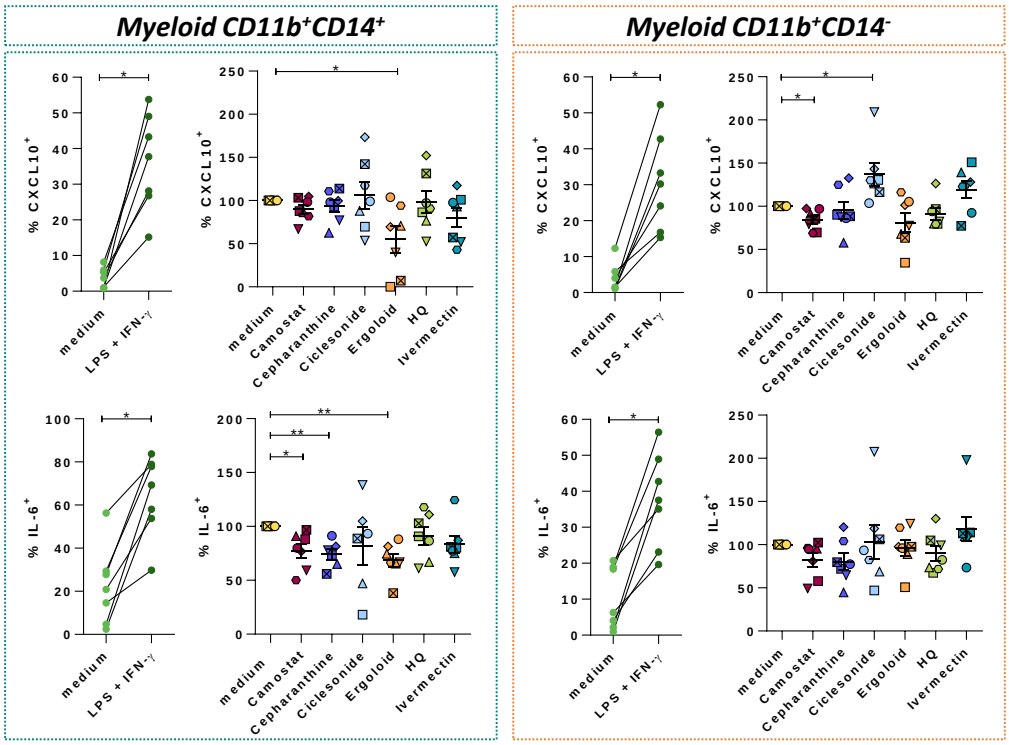
Myeloid CD11b+CD14+
Myeloid CD11b+CD14-
% CXCL10+
% IL-6+
medium
LPS + IFN-γ
Camostat
Cepharanthine
Ciclesonide
Ergoloid
HQ
Ivermectin